Arabian Journal of Geosciences (2020) 13: 168
https://doi.org/10.1007/s12517-020-5152-z

ORIGINAL PAPER

Soil moisture estimation in the transition zone from the Chengdu Plain region to the Longmen Mountains by field measurements and LANDSAT 8 OLI/TIRS-derived indices

Wenfu Peng [1,2] · Juan Wang [1,2] · Jie Zhang [1,2] · You Zhang [1,2]

Received: 17 October 2018 / Accepted: 22 January 2020 / Published online: 6 February 2020
© Saudi Society for Geosciences 2020

Abstract
Soil moisture is a key element in hydrological processes, and the accessibility of the moisture in the soil controls the mechanisms thereof amid land surface and atmospheric progressions. Many studies have examined the role of the land surface temperature (LST) and normalised difference vegetation index (NDVI) in changes in soil moisture. Nevertheless, an understanding of the influence of the temperature vegetation dryness index (TVDI), which combines the LST and the NDVI, on soil moisture remains elusive, including in the transition zone area from the Chengdu Plain region to the Longmen Mountains (TZ). In this study, the TVDI was calculated based on the NDVI and LST, using LANDSAT 8 operational land imager/thermal infrared sensor (OLI/TIRS) images. From the TVDI, regression models were trained by using 96 observation points of in situ soil moisture measurements to calculate the soil moisture in the transition zone. The results revealed that there is a strong and significant negative correlation between the TVDI and the in situ measured soil moisture ($P < 0.05$, $r = 0.710$, $R^2 = 0.504$). This indicates that the TVDI can reflect the soil moisture status in the TZ. The overall spatial patterns of soil moisture content were relatively high in the northwestern and central mountainous areas but were relatively low in the southeastern plains. Our study uniquely illustrates the spatial patterns of the relationship between TVDI variability and soil moisture variability in the TZ, western China and provides an approach for using remotely sensed soil moisture to optimise the parameterisation of soils in agricultural water management.

Keywords Soil moisture · Normalised difference vegetation index (NDVI) · Land surface temperature (LST) · Temperature vegetation dryness index (TVDI) · Remote sensing (RS) · Geographical information system(GIS)

Introduction

Soil moisture is a critical variable in many physical processes related to agriculture, hydrology, and meteorology or climatology (Maria Jose Escorihuela and Quintana-Seguí 2016; Wang et al. 2016). Assessments of soil moisture are especially significant for drought monitoring by agricultural industries and for observations of the ecological environment. In that regard, a great deal of attention has been paid to how changes in the land surface temperature (LST) and normalised difference vegetation index (NDVI) affect soil moisture. However, relatively less attention has been paid to how the temperature vegetation dryness index (TVDI), which is based on an empirical parameterisation of the relationship between LST and NDVI variations, impacts soil moisture. For example, the TVDI has not been studied in the area of the Longmen Mountains (TZ).

There are many different techniques for in situ soil moisture measurement (Skierucha and Wilczek 2010; Skierucha et al. 2012), but they are cost-intensive and require major efforts to be put in place (Chen et al. 2015). Moreover, only a few networks are available for in situ soil moisture measurement. Thus, remote sensing (RS) and geographical

Responsible Editor: Marouane Temimi

✉ Wenfu Peng
pwfzh@126.com

[1] The Institute of Geography and Resources Science, Sichuan Normal University, 7-2 mailbox, 1819, Chenglong Road, Longquanyi District, Chengdu 610101, Sichuan Province, People's Republic of China

[2] Key Lab of Land Resources Evaluation and Monitoring in Southwest, Ministry of Education, Sichuan Normal University, Chengdu, People's Republic of China

information system (GIS) are valuable spatiotemporal data and spatial analysis tools for soil moisture investigations (Chen et al. 2015; George P. Petropoulos et al. 2015).

Researchers in China and globally have investigated the impact of TVDI changes on soil moisture, owing to the availability of RS data of an areas over different time periods El Hajj et al. (2016). Watson et al. (1971) were the first to carry out a soil moisture inversion, using a model that combined the LST and thermal inertia. Sen and Yuan (2007) examined the relationship between the summer season NDVI and local-level climate variables, including precipitation and temperature in Minnesota from 1990 to 1997, using geographically weighted regression. Gao et al. (2011) presented a new drought assessment method that spatially and temporally integrated TVDI with a regional water stress index, based on a synergistic approach. Chen et al. (2011) investigated the potential of the TVDI for assessing soil moisture in the Huang-Huai-Hai plain from moderate resolution imaging spectroradiometer (MODIS) data. Chen et al. (2015) used the TVDI to investigate the differences in soil moisture under four types of mono-species forests and two types of mixed forests in Nanjing. Rébecca Filion et al. (2016) investigated the potential of radar and LANDSAT data in generating reliable soil moisture maps to support water management and agricultural practices in Mediterranean regions, particularly during dry seasons. Eftychia Taktikou et al. (2016) evaluated the capability of a soil water content predicted from RS to indicate the soil water content at a short time and space scale, through comparisons with daily soil moisture data determined in situ using dielectric devices. Wang et al. (2016) investigated the spatial distribution and limiting factors of the vegetation growth and NDVI change trends in two major alpine grasslands (alpine meadow and alpine steppe) in relation to soil temperature and soil water conditions, using datasets of the plateau scale soil water content, frozen soil type, vegetation index, and LST. A land parameter retrieval model was used to derive enhanced resolution soil moisture and vegetation optical depth data from advanced microwave scanning radiometer brightness temperatures, as sharpened by a modulation technique based on high-frequency observations (A.I. Gevaert et al. 2016). Comparisons with soil moisture from in situ measurements or model simulations indicated show that the TVDI is feasible for monitoring soil moisture (Chen et al. 2015).

Previous analyses indicated that soil moisture can be measured to some degree and have investigated the potential for obtaining the soil moisture through the relationship between the LST and NDVI, based on RS data. Although the findings from these studies are important, little research has focused on investigating the soil moisture in the ecologically fragile TZ, in western China. This research is important, both for helping us understand how the soil moisture and TVDI are linked over time and also for ensuring the assessment of the soil moisture. Therefore, this study investigates the suitability of RS data for estimating the soil moisture in the TZ.

The scale effects and cloud influence on optical RS data are very important scientific problems in RS (Chen et al. 2015) and can increase the uncertainty in soil moisture retrieval. LANDSAT 8 OLI/TIRS images have a higher spatial resolution (30–120 m) than Terra/Aqua MODIS images (250–1000 m) or National Oceanic and Atmospheric Administration-Advanced Very High Resolution Radiometer (NOAA-AVHRR) images (1100 m) where cloud cover affects the LST calculation and results in errors in the calculation. Therefore, this study uses good-quality images.

The objectives of this study are to (1) identify the distribution of the NDVI; (2) present the retrieved LST data based on atmospheric correction algorithms; (3) determine the suitability of the TVDI for estimating the soil moisture in the TZ; (4) estimate the soil moisture through RS data and establishment of the results with field measured soil moisture data.

Materials and methods

Study area

The study area is located in the northwest region of the Sichuan Basin between 103° 57′–104° 20′ E and 31° 15′–31° 41′ N (Fig. 1), in the transition zone between the Chengdu Plain region and the Longmen Mountains (TZ), and has a surface area of 79.48 km^2. The northwest section of the study area is a part of the TZ, whereas the southeast section of the study area is a part of the Chengdu Plain. Thus, the terrain is high in the northwest section and low in the southeast section, and there is a large difference in altitude between these sections. The study area lies in the subtropical humid climate zone of the Sichuan Basin and has a mild climate, abundant precipitation, and four distinct seasons, i.e. typical characteristics of the continental monsoon climate. The average annual temperature is 15.7 °C, and the average annual precipitation is 1053.2 mm. The distribution of vegetation in the region exhibits a distinct vertical gradient, owing to terrain and climate effects.

Data sources

The main types of research data in this study included RS data, field measured soil moisture data, and auxiliary data. The RS data included LANDSAT-8 OLI/TIRS RS images taken on 28 April 2016, with track number 129/038. The RS data was acquired from the 'US Geological Survey Earth Resources Observation and Science' data centre (USGS EROS Data Center), and a digital elevation model (DEM) was acquired from the Data Center for Resources and Environmental

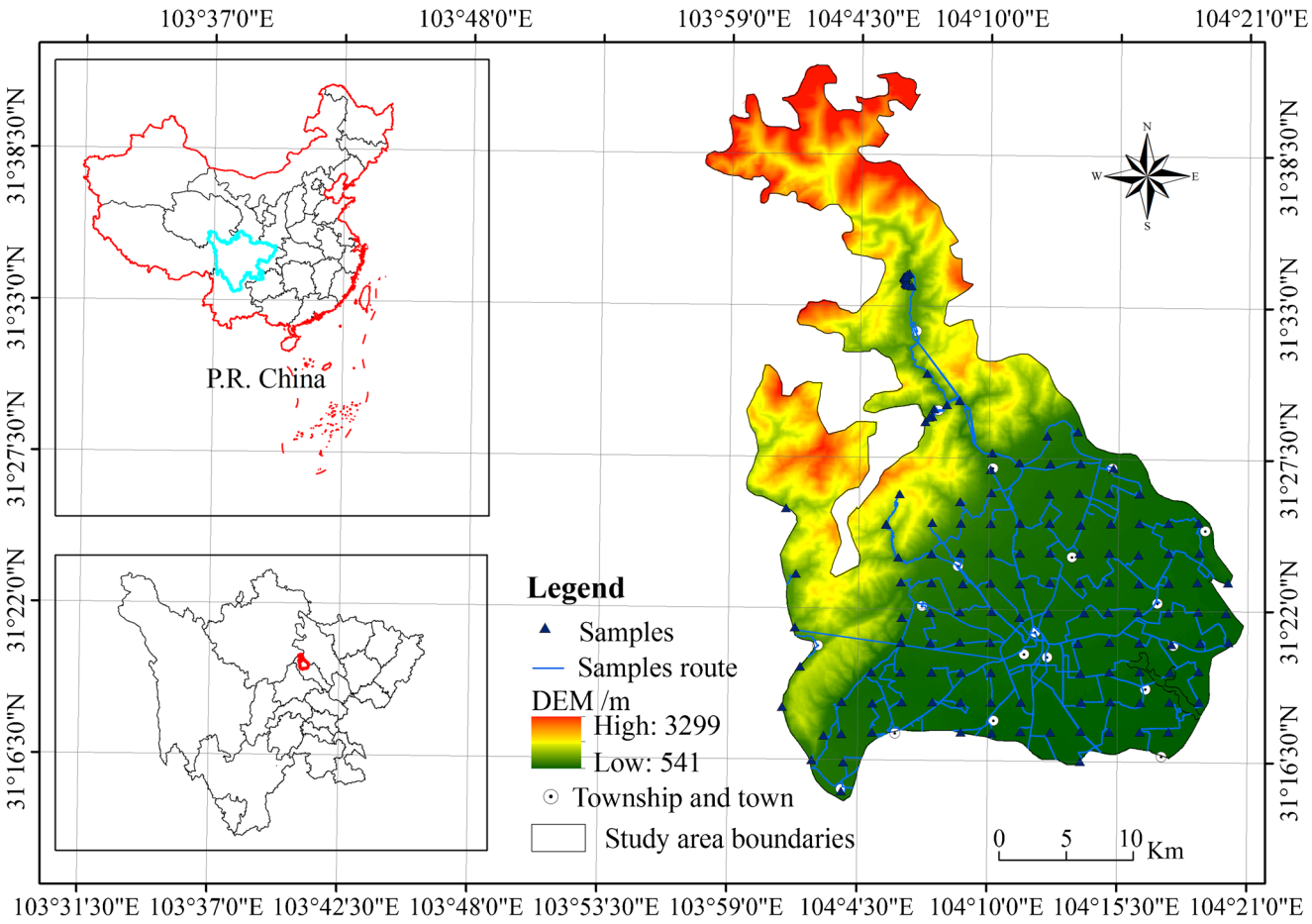

Fig. 1 Location of study area

Sciences, Chinese Academy of Sciences (RESDC), the Institute of Remote Sensing and Digital Earth, Chinese Academy of Sciences. The auxiliary data included 1:50,000 topography maps and vector boundary data for the study area, which were all obtained from a key lab of land resources evaluation and monitoring in the Southwest, Ministry of Education, i.e. Sichuan Normal University, while Global Positioning System (GPS) sampling data were obtained via field surveys.

Field work and soil samples processing

The field measured data was collected within a week before and after the RS imaging time, by handheld GPS devices. The weather was stable during the field work, and it could be determined that the soil moisture remained relatively stable. One hundred and twenty-four soil observation points of in situ soil moisture measurements were selected to ensure that each land use types had at least ten observation points (Fig. 1). However, cloud cover seriously influences LST retrieval and often limits the applicability of the TVDI for estimating soil moisture on a regional scale. Ninety-five effective field measured data points were retained using data exploration and elimination of abnormal values, such as the large errors caused in soil sampling or sample processing, points seriously influenced by cloud cover as determined based on GIS and Statistical Package for the Social Sciences software.

Previous results have shown that in the root zone of the soil profile, the relationships between the TVDI and soil moisture at depths of 0–20 cm in the soil samples were closer than those at depths (Patel et al. 2009; Chen et al. 2011; Sun et al. 2012;). The sampling depth in this study was approximately 20 cm, and each soil sample was crumbled before being placed in an aluminium box with a known accurate mass. Each sampling point was geo-referenced using a handheld GPS system. Samples were placed inside an oven preheated to 105 °C ± 2 °C and were then baked for 12 h. After removal and cooling to room temperature, each fresh soil sample was then immediately weighed to an accuracy of 0.001 g. For each sampling point, three measurements were made for the purpose of parallel determination. If there were significant discrepancies between the measurements for the first parallel sample, another round of drying would be carried out before re-weighing.

The main task during the field study was to measure the soil moisture using a direct method. The dried soil samples

were weighed using a Mettler balance, and the percent gravimetric soil moisture was calculated using Eq. (1):

$$M_s = \left(W_t - D_y\right)/D_y \times 100 \quad (1)$$

where the M_s, W_t, and D_y were soil moisture, soil wet weight, and soil dry weight, respectively.

Remote sensing processing

The RS data were projected using the Gauss–Krüger projection and were referenced to the World Geodetic System-84 coordinate system. The geometric corrections were performed on the 2016 RS images (using the 1:50,000 topographical maps) to create the reference image.

The 'Environment for Visualizing Images' (ENVI) software offers quick atmospheric correction (QUAC) and 'Fast Line-Of-Sight Atmospheric Analysis of Hypercubes' (FLAASH) atmospheric correction tools. QUAC is an atmospheric correction method for multispectral and hyperspectral imagery that works with the visible and near-infrared spectra in the shortwave infrared wavelength range. FLAASH is a first-principles atmospheric correction tool that corrects wavelengths in the visible spectrum through the near-infrared and shortwave infrared regions and can correct images collected in either vertical or slant-viewing geometries. The atmospheric correction of the LANDSAT 8 OLI/TIRS images in this study is accomplished using the ENVI 5.1 FLAASH model, which is based on the 'MODTRAN4 RT' model (French and Norman 2003).

The maximum likelihood method and GPS field data were used for the supervised classification of the 2016 images. The GPS field information was used to compare validation points to evaluate the accuracy of the determined land use types. The overall classification accuracy was above 90%, with a kappa coefficient of 0.856 or higher. Land use information was obtained on farmlands, forested lands, grasslands, water bodies, built-up land, and unused lands (Fig. 2).

The areas of each land cover types in the study area are presented in Table 1. According to Table 1, the land use was dominated by forested lands and farmlands, and these land types accounted for 83% or more of the study area. The data regarding the dependence of the land use landscape patterns on the elevation in the study area were obtained through spatial superposition analysis and statistical analysis of the land use maps and elevations. The results showed that cultivated lands, built-up land, and water areas were primarily distributed within the 535~854-m elevation range, and the proportion of the corresponding surface area in the study area was occupied more than 48%. The forested areas were mainly distributed in the 854~3299-m elevation range, and the proportion of the surface area in the study area was 38.47%. The unused lands were mainly distributed in the 854~2209-m elevation range.

Calculation of NDVI

The NDVI is an appropriate indicator for vegetation growth status, biomass, and vegetation coverage (Liang et al. 2012). It ranges from −1 to 1. Negative values indicate that the ground is covered by clouds, water, or snow, and thus, reflects visible light; 0 indicates the presence of rocks or bare soils, with the near-infrared and red bands being approximate or equal; and the positive values indicate the presence of vegetation cover, with the value increasing with greater coverage. The NDVI was calculated using the following Eq. (2):

$$\mathrm{NDVI} = (\mathrm{NIR} - R)/(\mathrm{NIR} + R) \quad (2)$$

where the NIR and R are the near-infrared band and red band reflectance values, respectively.

After an atmospheric correction of the results, some pixel values would become negative. This means that outliers beyond [−1,1] existed among the NDVI values. To facilitate calculations, the background for the NDVI values of these pixel values was set as 0 (Peng et al. 2016). The outliers were eliminated using Band Math in ENVI 5.1, yielding the processed NDVI data: (NDVI *lt* −1) × 0 + (NDVI *gt* 1) × 0 + (NDVI *ge* −1 and NDVI *le* 1) × NDVI

where the *lt* denotes 'less than', *gt* denotes 'greater than', denotes 'less than or equal to', and *ge* denotes 'greater than or equal to'.

Retrieval of fractional vegetation covers

A pixel binary model was used to determine the fractional vegetation covers (FVC). The NDVI value of a mixed pixel is formed by two components: areas with vegetation cover ($\mathrm{NDVI_{veg}}$) and those with bare soil/no vegetation cover ($\mathrm{NDVI_{soil}}$) (Zhao 2003). The FVC is calculated using the following Eq. (3):

$$\mathrm{FVC} = \left(\mathrm{NDVI} - \mathrm{NDVI_{soil}}\right)/\left(\mathrm{NDVI_{veg}} - \mathrm{NDVI_{soil}}\right) \quad (3)$$

where the $\mathrm{NDVI_{veg}}$ represents the NDVI values of the pure vegetation cover pixels, and $\mathrm{NDVI_{soil}}$ represents the NDVI value of the bare soil cover pixels.

The NDVI value of a pixel is affected by various factors, including the atmosphere, surface conditions, year, season, and regional conditions. These cause $\mathrm{NDVI_{soil}}$ and $\mathrm{NDVI_{veg}}$ to vary over space and time. For the calculation of NDVI values in this study, the confidence interval was set to 5% and 95% of the cumulative probability distribution table for the region's NDVI values. The NDVI values in the vicinity of 5% and 95%, specifically 0.003794 and 0.773399, were selected as the $\mathrm{NDVI_{soil}}$ and $\mathrm{NDVI_{veg}}$, values, respectively.

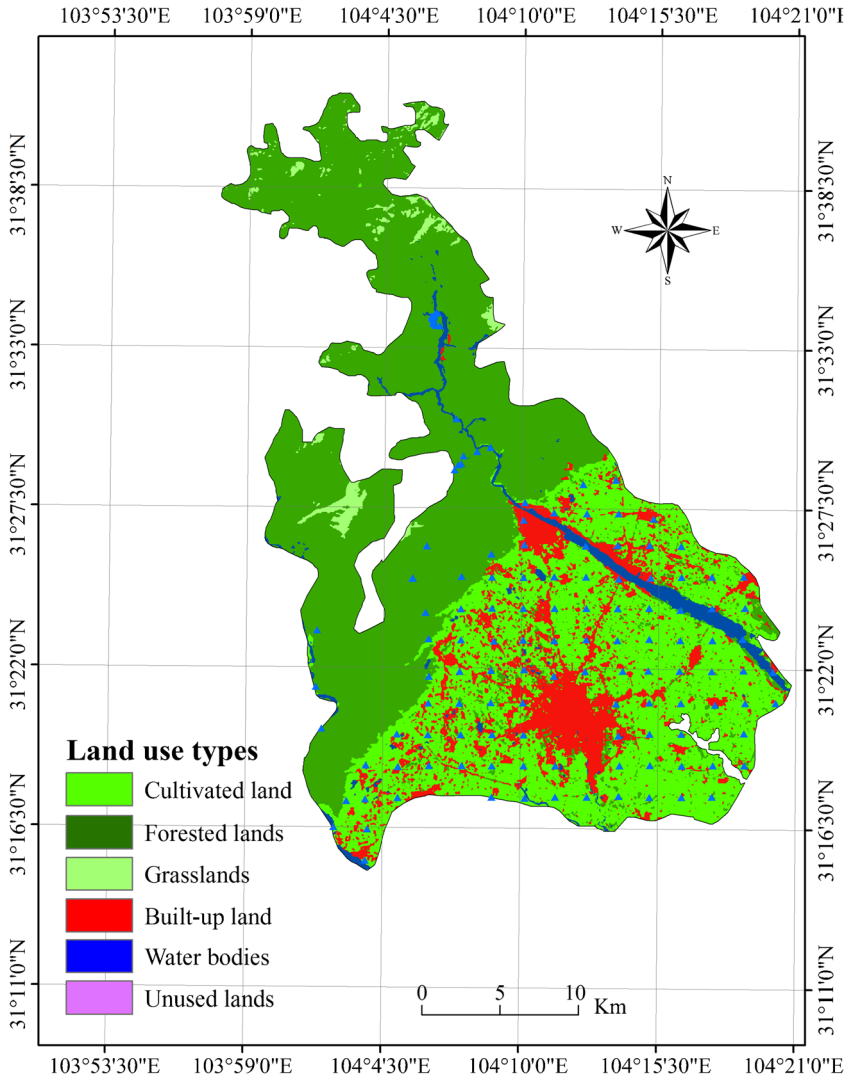

Fig. 2 Land use patterns in study area

Retrieval of the land surface temperature

Currently, the algorithms used for the RS retrieval of LST include the atmospheric correction algorithms (Sobrino et al. 2004; Li et al. 2004; Mao et al. 2005), single-window algorithms (Qin et al. 2001; Jiménez-Muoz et al. 2014; Zhou et al. 2011), and split-window algorithms (Wan and Dozier 1996; Ri et al. 2013). The LANDSAT 8 OLI/TIRS contains two thermal infrared bands: the band10 (10.60~11.19 μm) and band11 (11.50~12.51 μm). The US Geological Survey (USGS) has pointed out that some calibration errors can be found with the band 11. It is recommended to use only the TIRS band 10 in quantitative research rather than using two channels (Gao et al. 2017). As LANDSAT 8 OLI/TIRS 10 data is located at a lower atmospheric absorption band than TIRS11, its atmospheric transmissivity is higher, making it more suitable for single-band inversions of the LST (Jiménez-Muoz et al. 2014; Yu et al. 2014). The main difference between the single-window and single-channel algorithms is that in terms of atmospheric parameters, the former requires both near-surface temperatures and atmospheric moisture content, whereas the latter only requires atmospheric moisture content. Hence, the LANDSAT 8 OLI/TIRS 10 data and atmospheric correction method were adopted in this study for the inversion of the LST.

Table 1 The areas of each land cover types

Land use types	Area (units: ha)	Proportion (units: %)
Forest land	38,271.42	48.152
Water body	2299.95	2.894
Cultivated land	28,212.93	35.497
Built-up land	9459.63	11.902
Grass land	1233.09	1.551
Unused land	3.15	0.004

The atmospheric correction algorithms for calculating the LST were as follows: first, the atmospheric effect on surface

thermal radiation was estimated; second, this atmospheric impact was subtracted from the total thermal radiation observed by satellite sensors, and the surface thermal radiation intensity was obtained; finally, the thermal radiation intensity was converted to the corresponding LST.

Land surface emissivity

According to previous studies (Qin et al. 2004; Sobrino et al. 2004), the calculation process for land surface emissivity is as follows: first, the RS image is divided into town, water, and natural surface; second, the land surface emissivity values of the natural surface and towns are calculated based on the FVC. The emissivity value of the water is 0.995 because water continuity is strong and has fewer mixed pixels (Qin et al. 2004); the land surface emissivity values of the natural surface and towns are calculated based on the FVC as follows:

$$\varepsilon_{sf} = 0.9625 + 0.0614\mathrm{FVC} - 0.0461\mathrm{FVC}^2 \quad (4)$$

$$\varepsilon_{bd} = 0.9589 + 0.086\mathrm{FVC} - 0.0671\mathrm{FVC}^2 \quad (5)$$

where ε_{sf}, ε_{bd} are the emissivity values of the cities and towns, and natural surfaces, respectively, and FVC is the fractional vegetation cover of a pixel.

The ground radiation brightness

The thermal infrared radiation brightness is calculated as follows:

$$B(T_s) = \left[L_\lambda - L^{\uparrow} - \tau(1-\varepsilon) \times L_{\downarrow}\right]/\tau \times \varepsilon \quad (6)$$

where the $B(T_S)$ is the radiation brightness values in the thermal infrared band of a blackbody ($\mathrm{Wm^{-2}sr^{-1}\mu m^{-1}}$), L_λ is the thermal infrared radiation brightness value, $L^{\uparrow}$is the upwelling atmospheric radiance ($\mathrm{Wm^{-2}sr^{-1}\mu m^{-1}}$), $L^{\downarrow}$ is the down welling atmospheric irradiance divided by π ($\mathrm{Wm^{-2}sr^{-1}\mu m^{-1}}$), ε is the land surface emissivity, and τ is the total atmospheric transmittance along the path between the land surface and the satellite sensor. The imaging time and the centre latitude and longitude information were obtained from the official website of NASA (http://atmcorr.gsfc.nasa.gov/) and were used to determine the τ, $L^{\uparrow}$, and $L^{\downarrow}$ values as 0.76, 1.79 and 2.98 $\mathrm{Wm^{-2}sr^{-1}\mu m^{-1}}$, respectively.

LST

The inverse function of the Plank formula and the thermal infrared radiation brightness values was used to calculate the LST (Sospedra et al., 1998). Thermal radiances were converted to corresponding luminance temperatures, according to Planck's law. The temperature value was calculated in Kelvin (T_s) or Celsius from the above processes, as follows:

$$T_s = k_2 / \left[\ln \frac{k_1}{B(T_s)} + 1\right] \quad (7)$$

$$\mathrm{LST} = k_2 / \left[\ln \frac{k_1}{B(T_s)} + 1\right] - 273.5 \quad (8)$$

where T_s is the effective at-satellite brightness temperature in Kelvin (K), the LST is the land surface temperature in Celsius (°C), and k_1, k_2 for LANDSAT 8 OLI/TIRS are constant values of 774.8853 W/($\mathrm{m^2}$. Mm.sr) and 1321.0789 K, respectively.

Calculation of the temperature vegetation dryness index

The TVDI is a method for land surface soil moisture retrieval based on the optical and thermal infrared RS channel data (Sandholt et al. 2002). Therefore, the TVDI was used to estimate the soil moisture in the TZ. If an image contains a large space of soil moisture and green vegetation, the space presents a triangle. The triangle forms because the LST decreases as the vegetation cover increases. The scatter plot between the NDVI and LST is termed as the LST_NDVI space and is closely associated with surface evapotranspiration and moisture Amani et al. (2016).

Any random NDVI value corresponds to a set of dry and wet edges. The maximum LST decreases as the NDVI increases along the x-axis on the dry edge (Sandholt et al. 2002), and the stomatal resistance to evapotranspiration is a key factor, which is partly controlled by the limited moisture availability (Sandholt et al. 2002; Chen et al. 2015). The wet edge consists of a group of points forming a horizontal line. The LST is independent of the NDVI on the wet edge, and for the points closer to the wet edge, the evapotranspiration capacity and soil moisture become higher (Chen et al. 2015).

The computation formula was calculated as follows (Sandholt et al. 2002):

$$\mathrm{TVDI} = \frac{\mathrm{LST} - \mathrm{LST_{min}}}{\mathrm{LST_{max}} - \mathrm{LST_{min}}} \quad (9)$$

where the $\mathrm{LST_{max}}$ and $\mathrm{LST_{min}}$ represent the maximum and minimum LST values when the NDVI equals a particular value, whereas LST represents the surface temperature of any random pixel.

After the LST_NDVI eigenspace has been simplified to a triangle, $\mathrm{LST_{max}}$ and $\mathrm{LST_{min}}$ were concurrently subjected to linear regression:

$$\mathrm{LST_{min}} = a_1 + b_1 \times \mathrm{NDVI} \quad (10)$$

$$\mathrm{LST_{max}} = a_2 + b_2 \times \mathrm{NDVI} \quad (11)$$

where a_1,a_2 and b_1,b_2 are the intercepts and slopes of the dry

and wet edges, respectively, and the coefficients of the a_1,a_2 and b_1,b_2 can be determined by a least squares fit to the actual data, respectively.

Results and discussion

NDVI patterns

The NDVI values for the study area range from 0.00244 to 0.80481, and the overall spatial pattern shows a reduced NDVI from the TZ to plain region. The main land use type in the northwestern TZ region is woodlands, and the vegetation coverage is high. The NDVI values of the forest land and grassland in the mountain area are high. Some of the areas are affected by human activities. The main land use types are construction land, bare land, and water, where vegetation coverage is low. The NDVI values in the eastern plains are low. Hosseini and Saradjian (2011) studied four different soil water content estimation models, NDVI_LST, enhanced vegetation index (EVI)_LST, NDVI_LST_NDWI, and EVI_LST_NDWI; statistically, it was proven that when the EVI was replaced with the NDVI in the model, the accuracy of the soil moisture estimation increased (Fig. 3).

LST patterns

In summary, there was a significant decline in the LST from the plains to the mountainous areas (Fig. 4). The former is affected by the lower altitude and human activities, which caused higher temperatures. In that regard, a higher altitude may be an important factor for reducing LST, which, when combined with the reduced human activities in the mountainous areas and higher vegetation coverage, resulted in a relatively lower LST. There were abnormal inversion results owing to thick cloud covers.

The north western region of the study area is located in the TZ, and parts of the areas in the north western region

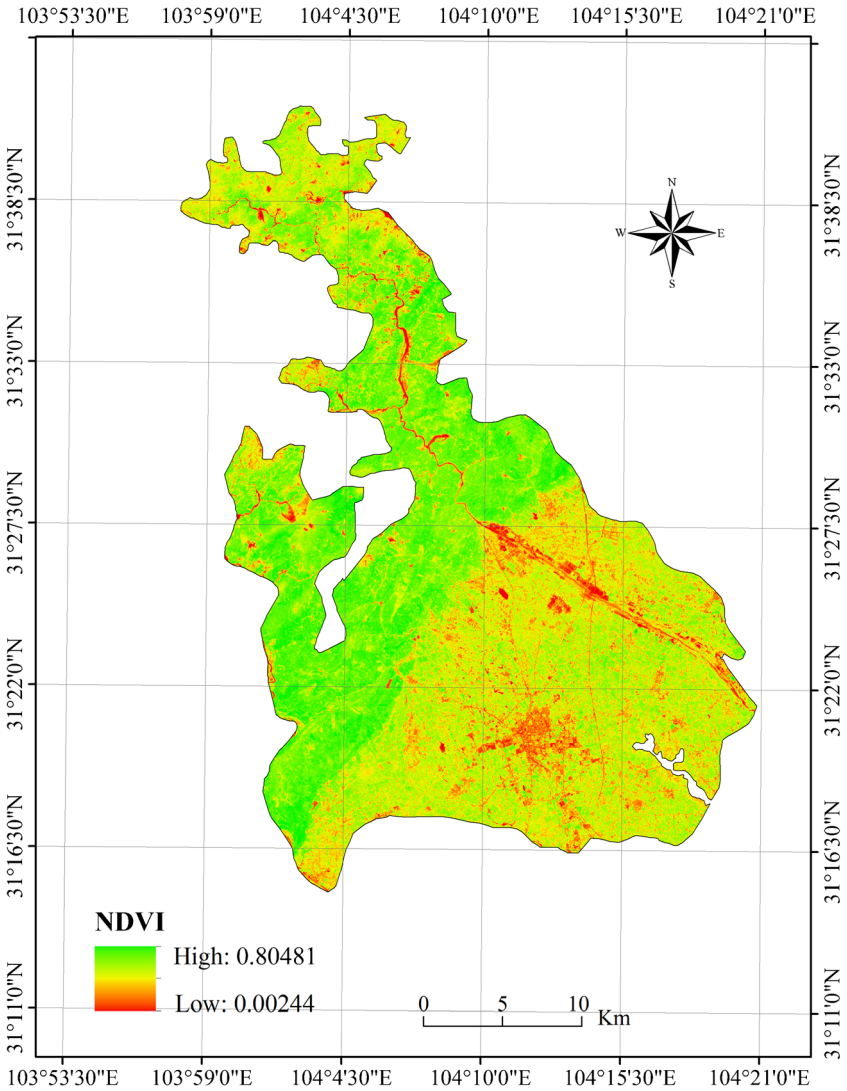

Fig. 3 Distribution of NDVI in study area

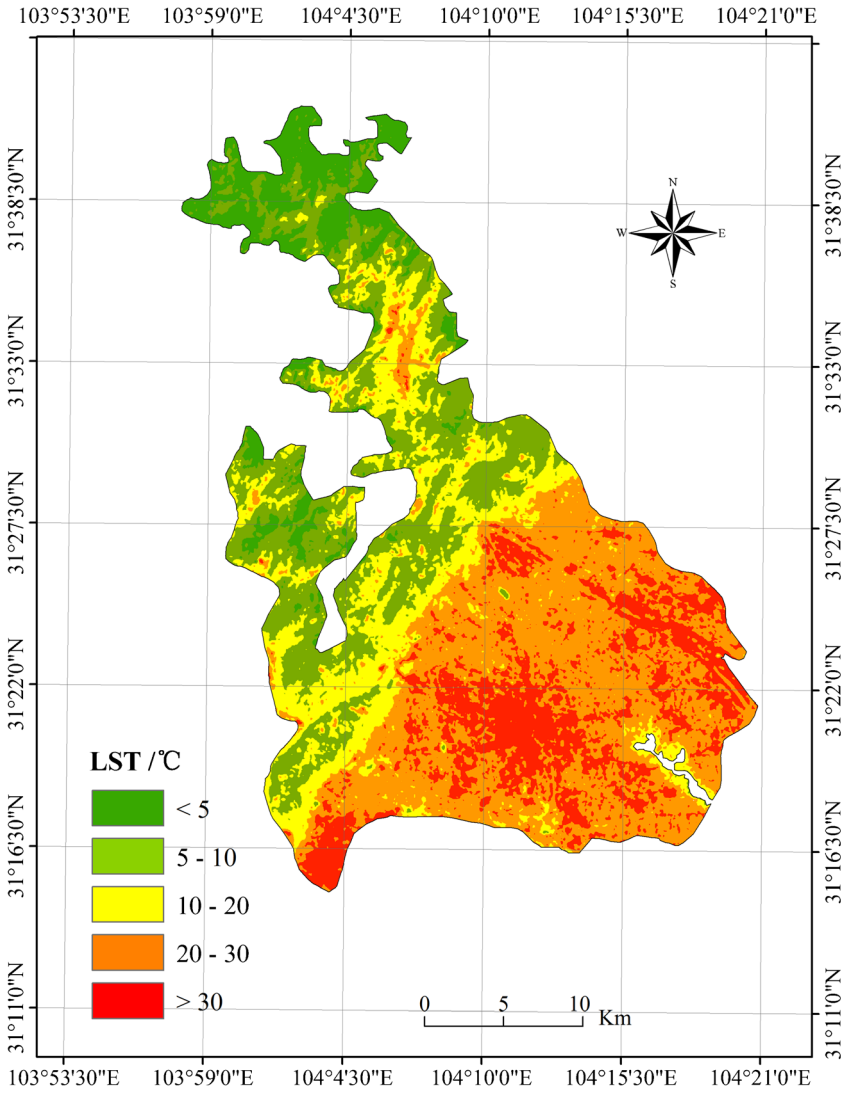

Fig. 4 Distribution of the average LST in study area

are covered by clouds. As a result, temperatures in these areas are below 5 °C. For areas not affected by cloud cover, a temperature range of 5~10 °C in the mountainous areas from April to May is considered normal. Temperatures in the central mountainous area, at 10~20 °C, are generally higher than those in the northwestern mountainous areas. The main land use type is woodlands, and the vegetation coverage is high. Some of the areas are affected by human activities or a slope direction/gradient, resulting in temperatures above 20 °C.

In the eastern plains, which are predominantly arable lands, the LST values are mostly near 20~30 °C. The central area of the plains is the main urban area, consisting mostly of lands for construction, the LST values there are 30~35 °C. According to the principle of the urban heat island effect, the LST values in cities are higher than those in surrounding areas. The LST even reached 35 °C and above in the middle of the urban area in study area. Field observations indicated the distribution of factories at these areas, and the higher LST values resulted from the industrial developments, emissions, and dense population distribution.

Analysis of the LST_NDVI eigen space

After setting the step size of the NDVI to 0.01, the EXCEL software and function calculations were used to extract the LST_{max} and LST_{min} values corresponding to the same NDVI value. The spatial scatter diagram of the LST_NDVI eigen space approximated a triangle (Fig. 5), which was similar to that in the description by Sandholt et al. (2002). The relationship between the NDVI and LST is near-linear. According to Fig. 5, the scatter tendency of the LST_{max} and LST_{min} can be divided into three segments:

When NDVI ≤ 0.15, the scatters for LST_{max} did not have a corresponding maximum value, whereas those for LST_{min} formed a straight line with a positive gradient;

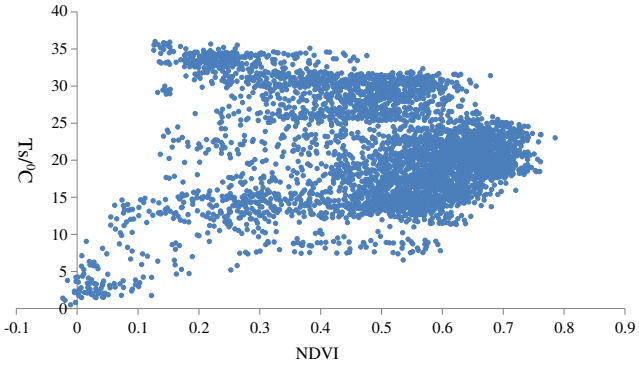

Fig. 5 LST_NDVI eigen space

When $0.15 < NDVI \leq 0.6$, the scatters for both LST_{max} and LST_{min} approximated horizontal straight lines with near-zero gradients; and,

When $0.6 < NDVI \leq 0.8$, the LST_{max} and LST_{min} lines were both straight, but with negative and positive gradients, respectively.

The plots of LST_{min} and LST_{max} as a function of NDVI are shown in Fig. 6. There was a strong correlation between the LST and NDVI. The *y*-axis represents the LST, and the *x*-axis shows NDVI (Fig. 5). The LST and NDVI relationship slope could be effectively determined during the growing season with a certain level of the NDVI. The derived LST/NDVI slope from the image windows was significantly correlated to the in situ soil moisture (Xin et al. 2006). With the increase in NDVI values, the LST values decreased, and vice versa.

The general trend of the dry and wet edges decreases and increases as with the NDVI value, respectively. Thus, LST_{max} decreases, but LST_{min} increases. To determine the parameters describing the dry and wet edges, the LST_{min} and LST_{max} values observed for small intervals of the NDVI are extracted in the LST_NDVI eigen space. The equations for the dry and wet edge for the three scenes are shown in Fig. 6.

Spatial variation of TVDI

The TVDIs of the TZ from the plain region to mountains were calculated, as shown in Fig. 7. According to Fig. 7, the spatial pattern variation of TVDI values has a significant reduction from the northwestern mountainous regions to southeastern plains area. The northwestern mountainous region has a high TVDI value, whereas the plain region has a low TVDI value owing to the different FVC values and human activities.

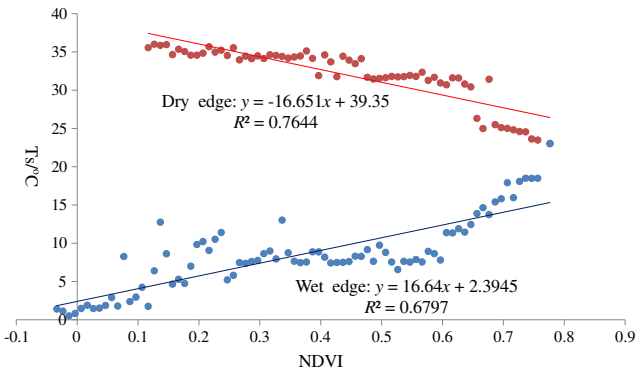

Fig. 6 Equations of LST_NDVI eigen space with dry edge and wet edge

Comparison of TVDI with in situ measurements

The effectiveness of the TVDI as an index for assessing soil moisture was validated by systematically designed in situ soil moisture measurements for each grid. The obtained TVDI value was compared with the measured soil moisture. Fifty-eight points were randomly selected for in situ soil moisture measurement to ensure that each land cover type had at least five observation points. There is a significant negative correlation between the TVDI and the in situ measured soil moisture ($R = 0.710$). Linear relationships exist between the soil moisture and the TVDI, NDVI, and LST (Table 2).

According to Table 2, all *P* values in the regression model were much less than 0.05. Therefore, the TVDI can reflect the soil moisture status better than the NDVI and LST. Patel et al. (2009) also revealed that a significantly strong and negative relationship exists between the TVDI and in situ soil moisture, particularly when the vegetation cover is sparse.

To verify the regression model accuracy, 38 points of in situ soil moisture measurement that were not involved in the model construction were used. The results show that the TVDI can reflect the soil moisture status. The root-mean-square error (RMSE) was 0.04897, and the *P* values were far less than 0.01. This proved that the accuracy of the soil moisture inversion was relatively high. The TVDI was also found to be satisfactory in capturing the temporal variation in the soil surface moisture status.

Researchers in China studies have used the TVDI to estimate soil moisture from different RS data and have produced different R^2 values (Chen et al. 2015; Bai et al. 2017). For example, in these different RS data, for NOAA-AVHRR images, $R^2 = 0.23–0.81$ (Goward et al. 2002; Wang et al. 2004); for Terra/Aqua MODIS images, $R^2 = 0.12–0.83$ Chen et al. (2012), and for LANDSAT TM images, calculated R^2 values is $R^2 = 0.15–0.80$ (Chen et al. 2015) etc. The R^2 values between the TVDI and soil moisture are still low in some studies (Chen et al. 2011; Chen et al. 2012). This is owing to scaling effects in the TVDI values retrieved from RS images. In that regard, each pixel in the LANDSAT TM image represents a grid of 30 m × 30 m, but each observation point of the in situ soil moisture measurement represents only a point on the soil surface. Thus, the in situ measured soil moisture

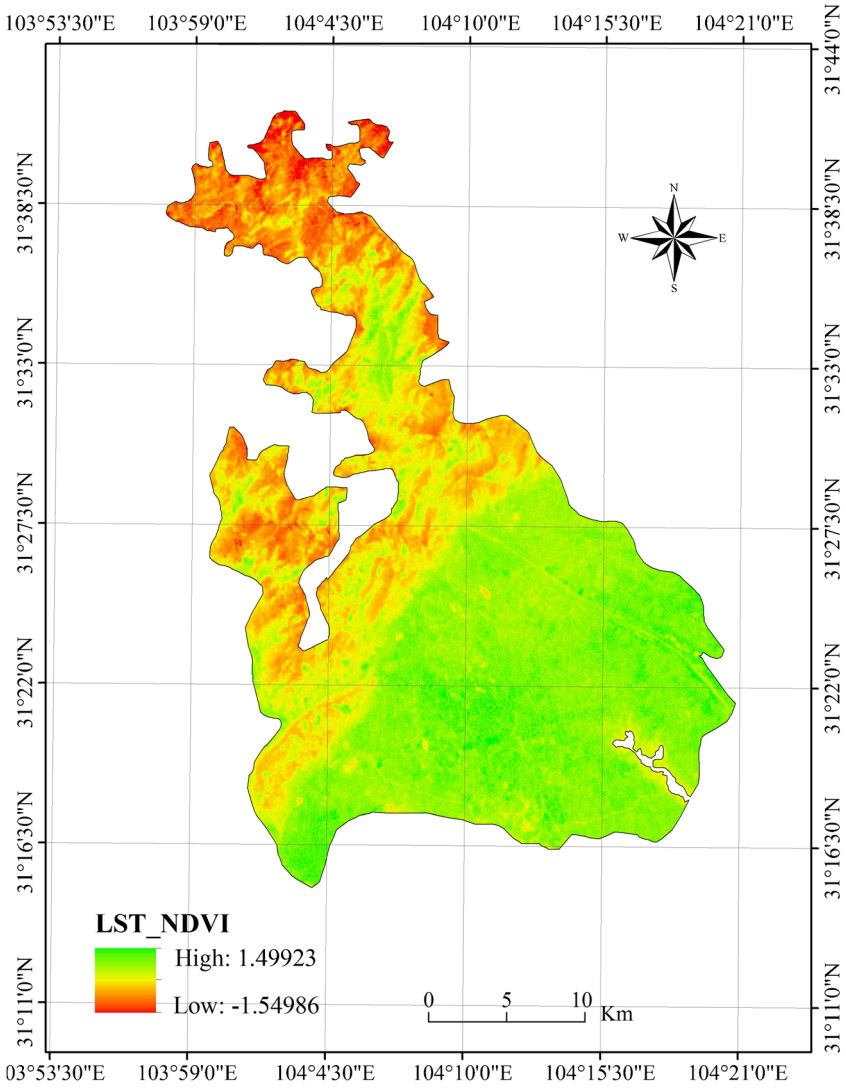

Fig. 7 Spatial distribution of TDVI in study area

cannot ensure a perfect match with the corresponding pixel in the image (Chen et al. 2015).

Spatial distribution of soil moisture

The spatial distribution of the soil moisture content within the study area based on the inversion results is shown in Fig. 8.

In terms of the overall distribution of the soil moisture content, the levels were relatively high in the northwestern and central mountainous areas but were relatively low in the southeastern plains. For areas within the TZ, a gradual decline in soil moisture levels was apparent from the plains towards the mountainous areas. This resulted from the general variation in soil moisture levels with altitudinal changes (535~3506 m), as well as the fact that the southeastern region of the study area sits on the plains of Chengdu and comprises predominantly arable lands and lands for construction, making it more affected by human activities. Second, although the northwestern and central regions of the study area are located in the mountainous areas and are subjected to less human impact, they are located on the Longmenshan seismic belt. Consequently, there are frequent mountain hazards, landslides, and debris flows. In addition, the 2008 earthquake had a major impact on the mountainous areas, making it difficult to restore the damaged vegetation cover. Nevertheless, gradual changes in the TZ's soil moisture levels may still be seen. Finally, the soil moisture content in localised areas was also affected by other factors such as the slope direction and land use type.

Table 2 Regression model of soil moisture

Regression model	Correlation coefficient	R^2	P
$y = -1.1249TVDI+1.1509$	0.710	0.5043	0.000
$y = 0.021\ NDVI+0.1988$	0.061	0.0037	0.000
$y = 0.0011LST+0.1809$	0.065	0.0029	0.019

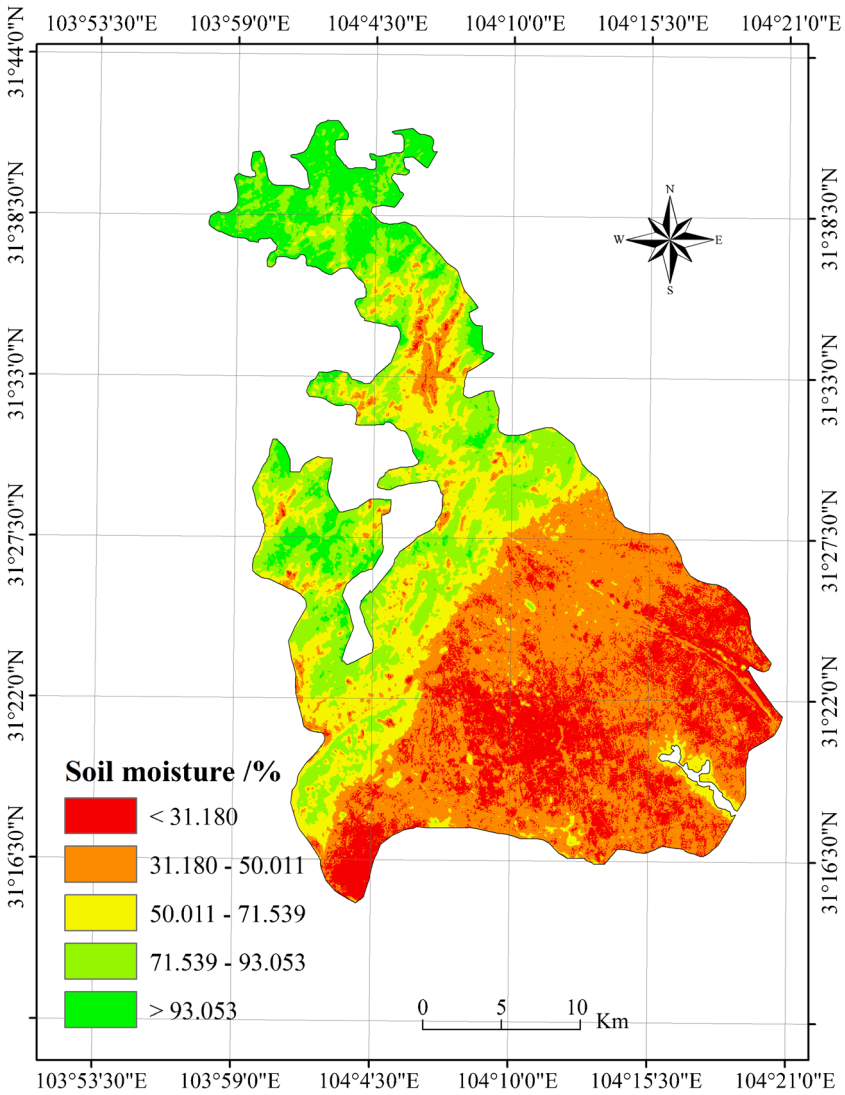

Fig. 8 Spatial distribution of soil moisture in study area

Conclusions

In this study, we examined how much of the soil moisture variability was associated with TVDI variability within and across the study area regions. A triangulation method was used to estimate the surface soil moisture. This method combines visible, infrared, and thermal data. The LST and NDVI values were obtained to derive TVDI values for the assessment of surface soil moisture through remotely sensed data and for the establishment of the results with field-measured soil moisture data. The method interpreted the pixel distribution in the LST_NDVI space. A triangle formed because the LST decreased as the vegetation cover increased. The scatter plot between the NDVI and LST is termed as the LST_NDVI space and is closely associated with surface evapotranspiration and moisture.

Our study is valuable in providing a spatially detailed account of where and by how much soil moisture varies and how much of this was driven by TVDI variability in the TZ. To a certain extent, this study supplements existing soil moisture research in a region with unique topographies, i.e. ranging from 535 to 3506 m. The soil moisture inversion of the study area contributes to the observation of changes in moisture levels as the plains transition towards the mountainous areas, and as arable lands transition towards woodlands. The results are of great significance for the monitoring of moisture content in arable lands and in the overall ecological environment.

We found a significant relationship between the TVDI and soil moisture at the observation points. Correlation and regression analyses were conducted to relate the TVDI to the in situ calculated soil moisture. The spatial pattern of the TVDI generally shows a low moisture distribution over the study area. A significant ($P < 0.05$) negative correlation of $r = 0.710$ was found between the TVDI and in situ soil moisture. The larger the TVDI value, the drier the soil; conversely, the higher the soil moisture levels, the smaller the TVDI values.

We found that the TVDI was adequate for the temporal variation of surface soil moistures. The TVDI provides a

consistent appraisal of the moisture situation. Consequently, it can be used to evaluate wet conditions. The accuracy of the soil water inversion in this study was high. For the study area, this proved the feasibility of using the TVDI for the soil moisture inversion. The soil moisture inversion was carried out at a depth of 20 cm over large areas throughout the study area. In the process, the calculation of the vegetation coverage was of vital importance. For the plains of Chengdu in particular, and the Sichuan Province in general, there have been very few studies with moisture inversions conducted based on the TVDI, nor have results been verified using measured data from field samples.

We thought that the effects of scaling might also have an impact on the accuracy of soil moisture and found that the appraisal of soil moisture using the TVDI was possible at medium spatial resolutions, as the relationship of soil moisture with LST and NDVI leads to an adequate number of representative pixels for developing a triangular scatter plot. The study area consisted predominantly of woodlands and arable lands, leading to high vegetation coverage. The LANDSAT 8 OLI/TIRS data selected for the study not only facilitated the calculation of the TVDI but also fully met the accuracy requirements for the soil moisture inversion. Our approach of using LANDSAT 8 OLI/TIRS data for temperature inversions based on the NDVI proved to be reliable and had a high resolution. However, cloud cover seriously influences the LST retrieval and often limits the applicability of the TVDI for estimating soil moisture on a regional scale.

Acknowledgements The authors thank the editors and anonymous referees for their valuable comments and suggestions, which helped improve the manuscript. LANDSAT data was acquired from the USGS EROS Data Center and the Institute of Remote Sensing and Digital Earth, Data Center for Resources and Environmental Sciences, Chinese Academy of Sciences (RESDC) (http://www.resdc.cn), Chinese Academy of Science.

Funding information Funding for this study was provided by the Humanities and Social Science Research Planning Foundation of National Ministry of Education of China (No. 17YJA850007) and National Natural Science Foundation of China (No. 41371125).

Compliance with ethical standards

Disclaimer The funding sources had no involvement in the collection, analysis, and interpretation of data; the writing of the report; and the decision to submit the article for publication.

References

Amani M, Parsian S, Mohammad S, Mazloumi M, Aieneh O (2016) Two new soil moisture indices based on the NIR-red triangle space of LANDSAT-8 data. Int J Appl Earth Obs Geoinf 50:176–186

Bai J, Yu Y, Di L (2017) Comparison between TVDI and CWSI for drought monitoring in the Guanzhong Plain, China. J Integr Agric 16(2):389–397

Chen SL, Liu YB, Wen ZM (2012) Satellite retrieval of soil moisture: an overview. Adv Earth Science 27:1192–1203

Chen S, Zuomin W, Hong J, Qingjian Z, Xiuying Z, Yan C (2015) Temperature vegetation dryness index estimation of soil moisture under different tree species. Sustainability 7:11401–11417

Chen J, Chunzhi W, Hong J, Liuxi M, Zhenrong Y (2011) Estimating soil moisture using temperature—vegetation dryness index (TVDI) in the Huanghuai-hai (HHH) plain. Int J Remote Sens 32(4):1165–1177

El Hajj M, Baghdadi N, Zribi M, Belaud G, Cheviron B, Courault D, Charron F (2016) Soil moisture retrieval over irrigated grassland using X-band SAR data. Remote Sens Environ 176:202–218

Escorihuela MJ, Quintana-Seguí P (2016) Comparison of remote sensing and simulated soil moisture datasets in Mediterranean landscapes. Remote Sens Environ 180:99–114

Filion R, Bernier M, Paniconi C, Chokmani K, Melis M, Soddu A, Talazac M, Lafortune F-X (2016) Remote sensing for mapping soil moisture and drainage potential in semi-arid regions: applications to the Campidano plain of Sardinia, Italy. Sci Total Environ 543(B):862–876

French AN, Norman JM, nderson MC (2003) A simple and fast atmospheric correction for spaceborne remote sensing of surface temperature. Remote Sens Environ 87:326–333

Gao WS, Zhang YZ, Fang SF, Ynag FJ, Wu H (2017) A fast estimation method of atmospheric parameters for LANDSAT-8 TIRS data. J Geo-inform Sci 19(1):110–116

Gao Z, Gao W, Chang NB (2011) Integrating temperature vegetation dryness index (TVDI) and regional water stress index (RWSI) for drought assessment with the aid of LANDSAT TM/ETM+ images. Int J Appl Earth Obs Geoinf 13(3):495–503

Gevaert AI, Parinussa RM, Renzullo LJ, van Dijk AIJM, de Jeu RAM (2016) Spatio-temporal evaluation of resolution enhancement for passive microwave soil moisture and vegetation optical depth. Int J Appl Earth Obs Geoinf 45(Part B):235–244

Goward SN, Xue YK, Czajkowski KP (2002) Evaluating land surface moisture conditions from the remotely sensed temperature/vegetation index measurements: an exploration with the simplified simple biosphere model. Remote Sens Environ 79:225–242

Hosseini M, Saradjian MR (2011) Multi-index-based soil moisture estimation using MODIS images. Int J Remote Sens 32(21):6799–6809

Jiménez-Muoz JC, Sobrino JA, Skokovic D, Mattar C, Cristóbal J (2014) Land surface temperature retrieval methods from LANDSAT-8 thermal infrared sensor data. IEEE Geosci Remote Sens Lett 11(10):1840–1843

Li FQ, Jackson TJ, Kustas WP, Schmugge TJ, French AN, Cosh MH, Bindlish R (2004) Deriving land surface temperature from LANDSAT 5 and 7 during SMEX02/SMACEX. Remote Sens Environ 92(4):521–534

Liang SL, Li XW, Wang JD (2012) Advanced remote sensing: terrestrial information extraction and applications. Academic Press, Pennsylvania

Mao KB, Qin ZH, Wang JM, Wu SL (2005) Lowtran retrieval of atmospheric water content and transmittance computation of MODIS bands 31 and 32. Remote Sensing Land Resources (1):26–29

Patel NR, Anapashsha R, Kumar S, Saha SK, Dadhwal VK (2009) Assessing potential of MODIS derived temperature/vegetation condition index (TVDI) to infer soil moisture status. Int J Remote Sens 30:23–39

Peng WF, Wang GJ, Zhou JM, Xu XL, Luo HL, Zhao JF, Yang CJ (2016) Dynamic monitoring of fractional vegetation cover along Minjiang River from Wenchuan County to Dujiangyan City using multi-temporal LANDSAT 5 and 8 images. Acta Ecol Sin 36(7):1975–1988

Petropoulos GP, Ireland G, Barrett B (2015) Surface soil moisture retrievals from remote sensing: current status, products & future trends. Phys Chem Earth 83–84(Parts A/B/C):36–56

Qin ZH, Karnieli A, Berliner P (2001) A mono-window algorithm forretrieving land surface temperature from LANDSAT TM data and its application to the Israel-Egypt border region. Int J Remote Sens 22(18):3719–3746

Qin ZH, Li WJ, Chen ZX, Xu B, Liu J (2004) The surface emissivity estimation of LANDSAT TM6 band. J Land Resources Remote Sensing (3):28–32

Ri C, Liu QH, Li H, Fang L, Yu YY, Sun DL (2013) Improved split window algorithm to retrieve LST from Terra/MODIS data.Journal of. Remote Sens 17(4):830–840

Sandholt I, Rasmussen K, Andersen J (2002) A simple interpretation of the surface temperature vegetation index space for assessment of surface moisture status. Remote Sens Environ 79(23):213–224

Skierucha W, Wilczek A (2010) A FDR sensor for measuring complex soil dielectric permittivity in the 10–500 MHz frequency range. Sensors 10:3314–3329

Skierucha W, Wilczek A, Szypłowska A, Sławiński C, Lamorski K (2012) A TDR-based soil moisture monitoring system with simultaneous measurement of soil temperature and electrical conductivity. Sensors 12:13545–13566

Sobrino JA, Jiménez-Muoza JC, Paolinib L (2004) Land surface temperature retrieval from LANDSAT TM 5. Remote Sens Environ 90(4): 434–440

Sen RS, Yuan F (2007) Patterns and variability of summer NDVI in response to climate variables at the local level in Minnesota. GISci Remote Sensing 44:166–181

Sun L, Sun R, Li X, Liang S, Zhang R (2012) Monitoring surface soil moisture status based on remotely sensed surface temperature and vegetation index information. Agric For Meteorol 166:175–187

Taktikou E, Bourazanis G, Papaioannou G, Kerkides P (2016) Prediction of soil moisture from remote sensing data. Procedia Engineering 162:309–316

Wang X, Yi S, Qingbai W, Yang K, Ding Y (2016a) The role of permafrost and soil water in distribution of alpine grassland and its NDVI dynamics on the Qinghai-Tibetan Plateau. Glob Planet Chang 147: 40–53

Wan ZM, Dozier J (1996) A generalized split-window algorithm for retrieving land-surface temperature from space. IEEE Trans Geosci Remote Sens 34(4):892–905

Wang CY, Qi SH, Niu Z, Wang JB (2004) Evaluating soil moisture status in China using the temperature–vegetation dryness index (TVDI). Can J Remote Sens 30:671–679

Watson K., Rowan L.,Offield T., 1971. Application of thermal modeling in the geologic interpretation of IR images (Thermal modeling for IR images geologic interpretation, discussing physical parameters role in materials natural environmental diurnal temperature behavior). International Symposium on Remote Sensing of Environment, 7th, University of Michigan, Ann Arbor, Mich, 2017–2041

Xin J, Tian G, Liu Q, Chen L (2006) Combining vegetation index and remotely sensed temperature for estimation of soil moisture in China. Int J Remote Sens 27(10):2071–2075

Yu XL, Guo XL, Wu ZC (2014) Land surface temperature retrieval from LANDSAT 8 TIRS-comparison between radiative transfer equation based method,split window algorithm and single channel method. Remote Sens 6(10):9829–9852

Zhao Y (2003) Analysis principle and method of remote sensing applications. Science press, Beijing, pp 1387–1398

Zhou J, Li J, Zhao X, Zhan WF, Guo JX (2011) A modified single-channel algorithm for land surface temperature retrieval from HJ-1B satellite data. J Infrared Millimeter Waves 30(1):61–67